Applied Physics Letters

Comparison of dielectric loss in titanium nitride and aluminum superconducting resonators

Cite as: Appl. Phys. Lett. **117**, 124004 (2020); https://doi.org/10.1063/5.0021950
Submitted: 15 July 2020 • Accepted: 05 September 2020 • Published Online: 23 September 2020

A. Melville, G. Calusine, W. Woods, et al.

Applied Physics Letters ARTICLE scitation.org/journal/apl

Comparison of dielectric loss in titanium nitride and aluminum superconducting resonators

Cite as: Appl. Phys. Lett. **117**, 124004 (2020); doi: 10.1063/5.0021950
Submitted: 15 July 2020 · Accepted: 5 September 2020 ·
Published Online: 23 September 2020

A. Melville,[1,a] G. Calusine,[1] W. Woods,[1] K. Serniak,[1] E. Golden,[1] B. M. Niedzielski,[1] D. K. Kim,[1] A. Sevi,[1] J. L. Yoder,[1] E. A. Dauler,[1] and W. D. Oliver[1,2,3]

AFFILIATIONS

[1]MIT Lincoln Laboratory, 244 Wood Street, Lexington, Massachusetts 02421, USA
[2]Research Laboratory of Electronics, Massachusetts Institute of Technology, Cambridge, Massachusetts 02139, USA
[3]Department of Electrical Engineering and Computer Science, Massachusetts Institute of Technology, Cambridge, Massachusetts 02139, USA

[a]Author to whom correspondence should be addressed: alexander.melville@ll.mit.edu

ABSTRACT

Lossy dielectrics are a significant source of decoherence in superconducting quantum circuits. In this report, we model and compare the dielectric loss in bulk and interfacial dielectrics in titanium nitride (TiN) and aluminum (Al) superconducting coplanar waveguide resonators. We fabricate isotropically trenched resonators to produce a series of device geometries that accentuate a specific dielectric region's contribution to the resonator quality factor. While each dielectric region contributes significantly to loss in TiN devices, the metal–air interface dominates the loss in the Al devices. Furthermore, we evaluate the quality factor of each TiN resonator geometry with and without a post-process hydrofluoric etch and find that it reduced losses from the substrate–air interface, thereby improving the quality factor.

Dielectric loss from material interfaces limits performance in superconducting quantum devices.[1–10] The magnitude of dielectric loss at these interfaces is determined by the materials and processes used to fabricate the devices. As such, it is imperative to develop a quantitative framework to understand how the loss at interfaces is affected by the choice of superconducting metal and subsequent fabrication steps. Significant work has focused on identifying which regions of a device may most strongly limit performance by modeling their electric field participation.[8,11,12] Separately, many reports have compared the performance of devices constructed using different materials or fabrication processes.[13–19] By combining these ideas, differences in the quality factor can be directly attributed to loss in specific dielectric regions, enabling further data-driven improvements to device performance.

In this work, we use the surface-loss extraction (SLE) process, outlined in Ref. 10, to model the dielectric regions of TiN and Al superconducting resonators and calculate the loss tangents of these regions based on the measured quality factors. We find that the metal–air interface of the Al resonators is an order of magnitude more lossy than that of TiN resonators. We also used a post-process HF etch to reduce the loss in the TiN devices and applied the SLE process to attribute the reduction specifically to the substrate–air interface.

We differentiate four dielectric regions from which we can extract a loss tangent (see Fig. 1): the metal–substrate (MS) interface, the substrate–air (SA) interface, the metal–air (MA) interface, and the silicon (Si) substrate. Two-level-system (TLS) defects in these dielectric regions limit the quality factor of a resonator to

$$Q_{\mathrm{TLS}}^{-1} = \sum_r p_r \tan\delta_r, \tag{1}$$

where p_r is the geometry-dependent electric field participation ratio and $\tan\delta_r$ is the loss tangent of dielectric region r. By measuring the intrinsic quality factor, Q_i, of a set of four specific resonator geometries with a distinct distribution of participation values, we numerically solved for the loss factor of each dielectric region,[10] which we then convert to a loss tangent using a reasonable set of assumptions about the dielectric constant and layer thickness.[20] The four geometries were each designed to accentuate participation in one of the four dielectric regions relative to the others. Therefore, we refer to the geometries as "MS design," "SA design," "MA design," and "Si design,"

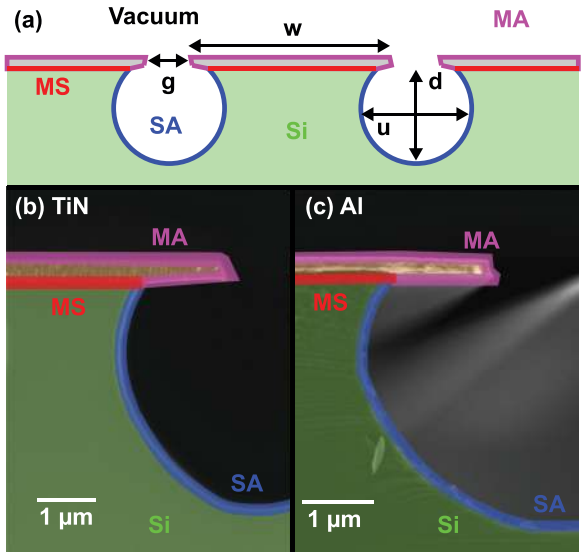

FIG. 1. (a) Diagram illustrating a cross section of a typical coplanar waveguide resonator with width (w), gap (g), trench depth (d), and degree of undercutting (u). The dielectric regions are labeled as follows: MS = metal–substrate interface, SA = substrate–air interface, MA = metal–air interface, and Si = silicon substrate. Representative cross-sectional scanning electron micrographs (SEMs) of deeply isotropically trenched TiN (b) and Al (c) resonators. The cross sections are used to generate a finite element model for calculating the participation ratio of each dielectric region.[21] Reprinted with permission from Woods *et al.*, Phys. Rev. Appl. **12**, 014012 (2019). Copyright 2019 American Physical Society.

corresponding to the dielectric region being emphasized. All geometries were isotropically trenched and coupled to the feedline with a coupling quality factor, Q_C, ranging from 0.15×10^6 to 5.0×10^6 to keep $Q_i \sim Q_C$ to avoid fitting errors. The trench depth (d) and degree of undercutting (u), along with the resonator width (w) and gap (g), set the interface participation ratios. For example, the MS design was shallowly trenched with a narrow width and gap, while the SA (Si) designs were deeply trenched with narrow (wide) widths and gaps. The MA design was deeply trenched with the resonator mostly suspended.[10]

All resonators were fabricated on high resistivity 8″ Si(001) substrates (>3500 Ω cm, Siltronic AG) that were prepared using the RCA clean prior to metal deposition. For the Al, the silicon wafers were also cleaned with an aqueous solution of 1% hydrofluoric acid (HF) to remove the native oxide prior to deposition. The 450 nm- or 750 nm-thick TiN films were deposited in a DC reactive-magnetron sputtering tool (background pressure $<2 \times 10^{-8}$ Torr), and the 250 nm-thick Al films were deposited in a molecular-beam epitaxy deposition tool (background pressure $<8 \times 10^{-11}$ Torr). The resonator patterns were defined with optical lithography, and the TiN metal was etched with a plasma formed from a combination of BCl_3 and Cl_2 gasses, whereas the Al metal was etched with a commercial acid etchant. After the resonator patterns were etched, we used an SF_6 plasma to isotropically etch the silicon trenches, which had the additional benefit of removing lossy Cl salts on the surface.[10,22] The increased thickness of the TiN resonators relative to the Al resonators was necessary to account for non-negligible etching of the underside of the TiN resonators due to the low selectivity of the SF_6 plasma etch between silicon and TiN. Since only the duration of the SF_6 plasma etch is varied between resonator designs, we assume that the loss tangent of each dielectric region in TiN is the same for all geometries. We similarly assume that the loss tangent of each dielectric region in Al is the same for all geometries.

An SEM cross section of each design was taken for each wafer used in this experiment, which is evident from the slightly different participation matrices used in the SLE process. In the case of Al, the chips with and without the post-process HF etch came from the same wafers and, thus, had the same participation matrix. After dicing, device chips for the post-process HF etch were etched with a 1% HF acid solution for approximately 30 s to strip the oxides from the surface and then rinsed with de-ionized water. All device chips were mounted in gold-plated copper packages. The HF-etched chips were loaded into the dilution fridge and pumped down to the millitorr range within 2–3 h of exposure to the atmosphere after the etch to minimize reformation of the native oxides.

The representative resonator chips were characterized by x-ray photoemission spectroscopy (XPS) before the post-process HF etch (orange line in Fig. 2) and approximately one hour after the post-process HF etch (blue line in Fig. 2). The delay between the post-process HF etch and the XPS scans approximates the time between the post-process HF etch and bringing the devices under vacuum in the dilution fridge. As expected, chlorine peaks are absent[22] and the oxygen peaks significantly diminished after the HF etch, indicating an effective removal of silicon oxide. In both the Al and TiN metal surfaces, the oxygen peaks were qualitatively unchanged, suggesting that the oxide was reformed faster than the timescale of the experiment.[23,24] Many previous reports have linked dielectric loss to surface oxides,[3,8,25] and so we expect that the observed decrease in surface oxides on silicon would result in a decreased substrate–air interface loss tangent after the post-process HF etch.

To determine the loss tangents, we measured between 10 and 50 resonators of each material and geometry, with and without the post-process HF etch, as a function of circulating microwave power to find the high power ($n_p \sim 10^6$) and single-photon power ($n_p \sim 1$) internal quality factors, Q_{HP} and Q_{LP}, respectively. The single-photon power is a common metric for the low-power regime in the community and

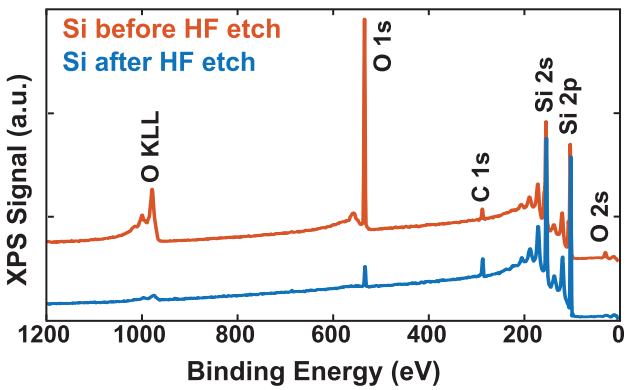

FIG. 2. X-ray photoemission spectroscopy (XPS) scan of a representative TiN resonator chip's silicon surface before (orange) and after (blue) the post-process HF treatment. The scans were offset to highlight the reduction in the intensity of the oxygen peaks resulting from the HF etch, indicating the removal of the native silicon oxide.

typically corresponds to a minimum value of the quality factor within our measurement error. The high-power metric was chosen to be the highest power at which the devices exhibited linear resonator behavior. For most devices, Q_{HP} was much larger than Q_{LP} such that $Q_{LP} \sim Q_{TLS}$. We used these to isolate the TLS-limited quality factor, Q_{TLS},[10,26] defined as

$$Q_{TLS}^{-1} = Q_{LP}^{-1} - Q_{HP}^{-1}. \quad (2)$$

Here, we neglect the temperature dependence of Q_{TLS}[1,15,17,27] because our experiments are fixed at $T_{base} = 25$ mK. We determined the loss tangent values, $\tan\delta_r$, by applying the SLE Monte Carlo simulation with N = 10 000, using each device set's participation matrix and the Q_{TLS} values.[10] The goodness-of-fit of the SLE process is shown in Fig. 3, where we plot the measured Q_{TLS} against the predicted Q_{TLS}. The y values correspond to the mean Q_{TLS} for each geometry, and the vertical error bars correspond to the standard error of the measured samples. The x values correspond to the mean Q_{TLS} calculated according to Eq. (1) using the participation matrix and the SLE loss tangents. The horizontal error bars are twice the standard deviation of the calculated quality factors.

The mean and standard deviation of the specific loss tangents determined by the SLE process are given in Table I, using the dielectric constants and thicknesses in Ref. 20. For some regions, e.g., the substrate–air interface for Al, the standard deviation of the loss tangent was much larger than the mean, which we interpreted as the loss tangent being too low to resolve due to the uncertainty in the SLE process given the accessible geometries. Our limited ability to deconvolve the participation of the MS or SA regions relative to the other dielectric regions is one source of uncertainty in the SLE process, which disproportionately affects the metal–substrate (MS) and substrate–air (SA) interfaces compared to the metal–air (MA) interface and the substrate (Si). We also observed greater uncertainty in the SLE process for dielectric regions that minimally affect the total device loss. These effects are apparent in the determination of the TiN substrate-air loss tangent after the post-process HF etch. In the cases where the loss tangent was obscured by the uncertainty, we report the upper bound of the loss tangent for these regions instead of the mean. The metal-substrate and substrate-air upper bounds were set by calculating the highest possible loss tangent consistent with the measured Q_{TLS} for the MS design and SA design, respectively.

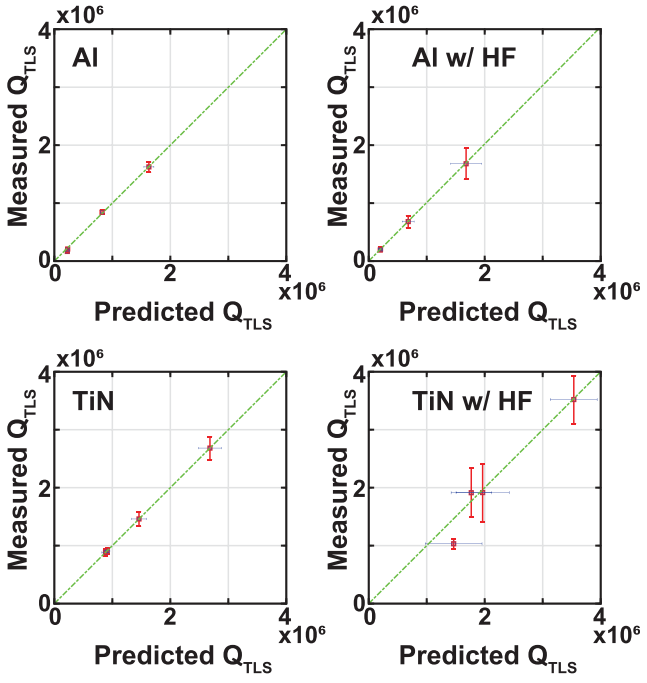

FIG. 3. For each test set, the measured Q_{TLS} is plotted against the Q_{TLS} calculated from the participation matrix and the model's loss tangents. Red vertical error bars correspond to the standard error of the measured Q_{TLS}, and blue horizontal error bars correspond to twice the standard deviation of the calculated quality factors. The green line represents perfect agreement between the measured Q_{TLS} and the predicted Q_{TLS}.

TABLE I. Loss tangents for the four dielectric regions by the material and process.

	Loss tangents			
Process	MS ($\times10^{-4}$)	SA ($\times10^{-3}$)	MA ($\times10^{-3}$)	Si ($\times10^{-7}$)
TiN	4.6 ± 2.4	1.7 ± 0.4	3.3 ± 0.4	2.6 ± 0.4
TiN w/HF	2.7 ± 3.0	<1.2	3.5 ± 1.2	2.8 ± 0.6
Al	<3.2	<2.9	29.4 ± 2.9	2.6 ± 0.8
Al w/HF	<1.3	<3.5	32.7 ± 3.6	1.3 ± 1.7

For both TiN and Al, we found that the loss tangent for the silicon dielectric region is the same within the error bars, as we expected given that (1) the properties of bulk silicon should not change from the fabrication process and (2) the silicon was sourced from the same vendor for all samples. The Si loss tangent we extract is also consistent with other values reported in the literature.[10–12] The most significant material-dependent difference was the loss tangent of the metal–air interface; it is an order of magnitude higher in Al than in TiN. We attribute this to a lossier and thicker aluminum oxide compared to the relatively thin oxide that forms on TiN.[10,24,27,28] While precise quantitative determination of the metal-substrate and substrate-air loss tangents was not possible in the Al devices, the upper bounds that we set are comparable to their counterparts in TiN without the post-process HF etch.

The only loss tangent that significantly changed due to the post-process HF etch was for the substrate–air interface in TiN, consistent with the expected reduction of silicon oxide at that interface. Although a similar reduction of oxides on the silicon surface occurred in the Al resonator chips from the post-process HF etch, the substrate-air loss tangent was already below the noise floor for Al without the post-process HF etch, and we would not expect to resolve changes to it. In Fig. 4, we plot the effect of the post-process HF etch for each geometry in TiN by comparing the total measured dielectric loss, Q_{TLS}^{-1}, with the calculated dielectric loss from the substrate–air interface. For most geometries, the observed reduction in loss is proportional to the participation ratio of the substrate–air interface. The most significant reductions were observed in the MS and SA designs, corresponding to a decrease in over 50% in the total measured dielectric loss and an increase in the overall device performance as determined by the single-photon power internal quality factor, Q_{LP}. The average Q_{LP} for

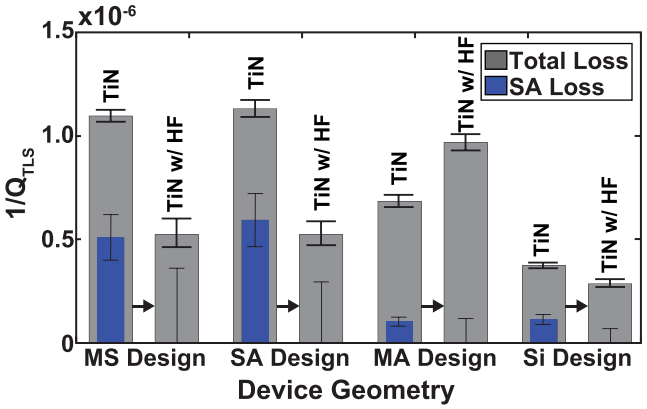

FIG. 4. The gray bars represent the measured dielectric loss (Q_{TLS}^{-1}) for each geometry for TiN, with and without the post-process HF etch. The blue bar within each segment represents the predicted loss ascribed to the substrate–air interface. The black arrows indicate the data corresponding to the effect of the post-process HF etch.

the MS and SA designs increased from 8.6×10^5 and 8.0×10^5 to 1.3×10^6 and 2.1×10^6, an increase in 50% and 160%, respectively, over the untreated devices. A similar reduction in loss was not observed for the MA design because the difference in the participation ratio due to the wafer-to-wafer etch variation between the TiN MA designs obscured the impact of the reduced substrate-air loss tangent on total dielectric loss in that geometry.

In summary, we demonstrated the use of the SLE process developed in Ref. 10 to quantitatively compare the dielectric loss of superconducting quantum devices made of different materials and fabrication processes. We found that the Al metal-air interface was ~10× lossier than the TiN metal–air interface. By characterizing the loss at different interfaces, we could strategically target a particularly lossy interface (SA) for improvement. We used a post-process HF etch to reduce the native oxide at that interface, which reduced the substrate-air loss tangent and resulted in more than a 2× increase in the single-photon quality factor compared to untreated devices for devices with the highest substrate–air participation.

See the supplementary material for the participation matrices used for the loss tangent extractions, for the XPS scans of the TiN and Al resonator surfaces, for a representative plot of the power dependent resonator behavior for the MS and SA designs both with and without the post-process HF etch, for the method for calculating the upper bounds in Table I, and for an analogous plot to Fig. 4 with the Al device geometries with and without the post-process HF etch.

AUTHORS' CONTRIBUTIONS

A.M., G.C., and W.W. contributed equally to this work.

We gratefully acknowledge M. Augeri, P. Baldo, M. Cook, R. Das, M. Hellstrom, V. Iaia, K. Magoon, P. Miller, P. Murphy, B. Osadchy, C. Stull, C. Thoummaraj, and D. Volfson at MIT Lincoln Laboratory for technical assistance. This material is based upon work supported by the Department of Defense under Air Force Contract Nos. FA8721-05-C-0002 and/or FA8702-15-D-0001. Any opinions, findings, conclusions, or recommendations expressed in this material are those of the authors and do not necessarily reflect the views of the Department of Defense.

DATA AVAILABILITY

The data that support the findings of this study are available upon reasonable request and with the permission of our US Government sponsors who funded the work.

REFERENCES

[1]J. M. Martinis, K. B. Cooper, R. McDermott, M. Steffen, M. Ansmann, K. D. Osborn, K. Cicak, S. Oh, D. P. Pappas, R. W. Simmonds, and C. C. Yu, "Decoherence in Josephson qubits from dielectric loss," Phys. Rev. Lett. **95**, 210503 (2005).
[2]J. Gao, B. Mazin, M. Daal, P. Day, H. LeDuc, and J. Zmuidzinas, "Power dependence of phase noise in microwave kinetic inductance detectors," Proc. SPIE **6275**, 627509 (2006).
[3]J. Gao, M. Daal, J. M. Martinis, A. Vayonakis, J. Zmuidzinas, B. Sadoulet, B. A. Mazin, P. K. Day, and H. G. Leduc, "A semiempirical model for two-level system noise in superconducting microresonators," Appl. Phys. Lett. **92**, 212504 (2008).
[4]A. D. O'Connell, M. Ansmann, R. C. Bialczak, M. Hofheinz, N. Katz, E. Lucero, C. McKenney, M. Neeley, H. Wang, E. M. Weig, A. N. Cleland, and J. M. Martinis, "Microwave dielectric loss at single photon energies and millikelvin temperatures," Appl. Phys. Lett. **92**, 112903 (2008).
[5]R. Barends, H. L. Hortensius, T. Zijlstra, J. J. A. Baselmans, S. J. C. Yates, J. R. Gao, and T. M. Klapwijk, "Contribution of dielectrics to frequency and noise of NbTiN superconducting resonators," Appl. Phys. Lett. **92**, 223502 (2008).
[6]M. R. Vissers, J. Gao, D. S. Wisbey, D. A. Hite, C. C. Tsuei, A. D. Corcoles, M. Steffen, and D. P. Pappas, "Low loss superconducting titanium nitride coplanar waveguide resonators," Appl. Phys. Lett. **97**, 232509 (2010).
[7]S. J. Weber, K. W. Murch, D. H. Slichter, R. Vijay, and I. Siddiqi, "Single crystal silicon capacitors with low microwave loss in the single photon regime," Appl. Phys. Lett. **98**, 172510 (2011).
[8]J. Wenner, R. Barends, R. C. Bialczak, Y. Chen, J. Kelly, E. Lucero, M. Mariantoni, A. Megrant, P. J. J. O'Malley, D. Sank, A. Vainsencher, H. Wang, T. C. White, Y. Yin, J. Zhao, A. N. Cleland, and J. M. Martinis, "Surface loss simulations of superconducting coplanar waveguide resonators," Appl. Phys. Lett. **99**, 113513 (2011).
[9]J. B. Chang, M. R. Vissers, A. D. Córcoles, M. Sandberg, J. Gao, D. W. Abraham, J. M. Chow, J. M. Gambetta, M. B. Rothwell, G. A. Keefe, M. Steffen, and D. P. Pappas, "Improved superconducting qubit coherence using titanium nitride," Appl. Phys. Lett. **103**, 012602 (2013).
[10]W. Woods, G. Calusine, A. Melville, A. Sevi, E. Golden, D. K. Kim, D. Rosenberg, J. L. Yoder, E. Dauler, and W. D. Oliver, "Determining interface dielectric losses in superconducting coplanar-waveguide resonators," Phys. Rev. Appl. **12**, 014012 (2019).
[11]C. Wang, C. Axline, Y. Y. Gao, T. Brecht, Y. Chu, L. Frunzio, M. H. Devoret, and R. J. Schoelkopf, "Surface participation and dielectric loss in superconducting qubits," Appl. Phys. Lett. **107**, 162601 (2015).
[12]J. M. Gambetta, C. E. Murray, Y. K. K. Fung, D. T. McClure, O. Dial, W. Shanks, J. W. Sleight, and M. Steffen, "Investigating surface loss effects in superconducting transmon qubits," IEEE Trans. Appl. Supercond. **27**, 1–5 (2017).
[13]R. Barends, J. J. A. Baselmans, J. N. Hovenier, J. R. Gao, S. J. C. Yates, T. M. Klapwijk, and H. F. C. Hoevers, "Niobium and tantalum high Q resonators for photon detectors," IEEE Trans. Appl. Supercond. **17**, 263 (2007).
[14]H. Wang, M. Hofheinz, J. Wenner, M. Ansmann, R. C. Bialczak, M. Lenander, E. Lucero, M. Neeley, A. D. O'Connell, D. Sank, M. Weides, A. N. Cleland, and J. M. Martinis, "Improving the coherence time of superconducting coplanar resonators," Appl. Phys. Lett. **95**, 233508 (2009).
[15]J. M. Sage, V. Bolkhovsky, W. D. Oliver, B. Turek, and P. B. Welander, "Study of loss in superconducting coplanar waveguide resonators," J. Appl. Phys. **109**, 063915 (2011).
[16]A. Megrant, C. Neill, R. Barends, B. Chiaro, Y. Chen, L. Feigl, J. Kelly, E. Lucero, M. Mariantoni, P. J. J. O'Malley, D. Sank, A. Vainsencher, J. Wenner,

T. C. White, Y. Yin, J. Zhao, C. J. Palmstrom, J. M. Martinis, and A. N. Cleland, "Planar superconducting resonators with internal quality factors above one million," Appl. Phys. Lett. **110**, 113510 (2012).
[17]A. Bruno, G. de Lange, S. Asaad, K. L. van der Enden, N. K. Langford, and L. DiCarlo, "Reducing intrinsic loss in superconducting resonators by surface treatment and deep etching of silicon substrates," Appl. Phys. Lett. **106**, 182601 (2015).
[18]A. P. M. Place, L. V. H. Rodgers, P. Mundada, B. M. Smitham, M. Fitzpatrick, Z. Leng, A. Premkumar, J. Bryon, S. Sussman, G. Cheng, T. Madhavan, H. K. Babla, B. Jack, A. Gyenis, N. Yao, R. J. Cava, N. P. de Leon, and A. A. Houck, "New material platform for superconducting transmonqubits with coherence times exceeding 0.3 milliseconds," preprint arXiv:2003.00024 (2020).
[19]I. Tsioutsios, K. Serniak, S. Diamond, V. Sivak, Z. Wang, S. Shankar, L. Frunzio, R. Schoelkopf, and M. Devoret, "Free-standing silicon shadow masks for transmon qubit fabrication," AIP Adv. **10**, 065120 (2020).
[20]We assumed the following thicknesses and dielectric constants to generate loss tangents: $t_{MS} = 2\,\text{nm}$, $t_{SA} = 2\,\text{nm}$, $t_{MA} = 2\,\text{nm}$, $\epsilon_{MS} = 11.4\epsilon_0$, $\epsilon_{SA} = 4\epsilon_0$, and $\epsilon_{MA} = 10\epsilon_0$.
[21]See www.comsol.com for information about COMSOL 5.4.
[22]M. Sandberg, M. R. Vissers, J. S. Kline, M. Weides, J. Gao, D. S. Wisbey, and D. P. Pappas, "Etch induced microwave losses in titanium nitride superconducting resonators," Appl. Phys. Lett. **100**, 262605 (2012).
[23]P. Dumas, J. Dubarry-Barbe, D. Riviére, Y. Levy, and J. Corset, "Growth of thin alumina film on aluminium at room temperature: A kinetic and spectroscopic study by surface plasmon excitation," J. de Phys. Colloques **44**(C10), 205–208 (1983).
[24]S. Ohya, B. Chiaro, A. Megrant, C. Neill, R. Barends, Y. Chen, J. Kelly, D. Low, J. Mutus, P. J. J. O'Malley, P. Roushan, D. Sank, A. Vainsencher, J. Wenner, T. C. White, Y. Yin, B. D. Schultz, C. J. Palmstrøm, B. A. Mazin, A. N. Cleland, and J. M. Martinis, "Room temperature deposition of sputtered tin films for superconducting coplanar waveguide resonators," Superconductor Sci. Technol. **27**, 015009 (2014).
[25]C. Mueller, J. H. Cole, and J. Lisenfeld, "Towards understanding two-level-systems in amorphous solids: Insights from quantum circuits," Rep. Prog. Phys. **82**, 124501 (2019).
[26]G. Calusine, A. Melville, W. Woods, R. Das, C. Stull, V. Bolkhovsky, D. Braje, D. Hover, D. K. Kim, X. Miloshi, D. Rosenberg, A. Sevi, J. L. Yoder, E. Dauler, and W. D. Oliver, "Analysis and mitigation of interface losses in trenched superconducting coplanar waveguide resonators," Appl. Phys. Lett. **112**, 062601 (2018).
[27]D. P. Pappas, M. R. Vissers, D. S. Wisbey, J. S. Kline, and J. Gao, "Two level system loss in superconducting microwave resonators," IEEE Trans. Appl. Supercond. **21**, 871–874 (2011).
[28]L. Gordon, H. Abu-Farsakh, A. Janotti, and C. G. Van de Walle, "Hydrogen bonds in Al_2O_3 as dissipative two-level systems in superconducting qubits," Nat. Sci. Rep. **4**, 7590 (2014).